Augmin shapes the anaphase spindle for efficient cytokinetic furrow ingression and abscission

Ryota Uehara[a,b,c,*], Tomoko Kamasaki[c,†], Shota Hiruma[a], Ina Poser[d], Kinya Yoda[c], Junichiro Yajima[b], Daniel W. Gerlich[e], and Gohta Goshima[c]

[a]Creative Research Institution, Hokkaido University, Sapporo 001-0021, Japan; [b]Department of Life Sciences, School of Arts and Sciences, University of Tokyo, Tokyo 153-8902, Japan; [c]Division of Biological Science, Graduate School of Science, Nagoya University, Nagoya 464-8602, Japan; [d]Max Planck Institute of Molecular Cell Biology and Genetics, 01307 Dresden, Germany; [e]Institute of Molecular Biotechnology of the Austrian Academy of Sciences, Vienna Biocenter Campus, 1030 Vienna, Austria

ABSTRACT **During anaphase, distinct populations of microtubules (MTs) form by either centrosome-dependent or augmin-dependent nucleation. It remains largely unknown whether these different MT populations contribute distinct functions to cytokinesis. Here we show that augmin-dependent MTs are required for the progression of both furrow ingression and abscission. Augmin depletion reduced the accumulation of anillin, a contractile ring regulator at the cell equator, yet centrosomal MTs were sufficient to mediate RhoA activation at the furrow. This defect in contractile ring organization, combined with incomplete spindle pole separation during anaphase, led to impaired furrow ingression. During the late stages of cytokinesis, astral MTs formed bundles in the intercellular bridge, but these failed to assemble a focused midbody structure and did not establish tight linkage to the plasma membrane, resulting in furrow regression. Thus augmin-dependent acentrosomal MTs and centrosomal MTs contribute to nonredundant targeting mechanisms of different cytokinesis factors, which are required for the formation of a functional contractile ring and midbody.**

Monitoring Editor
William Bement
University of Wisconsin

Received: Feb 23, 2015
Revised: Jan 5, 2016
Accepted: Jan 7, 2016

INTRODUCTION

After the onset of anaphase in animal cells, cytokinesis is accomplished through two consecutive processes: ingression of the cleavage furrow by contraction of the contractile ring, and abscission of the intercellular bridge that links the two daughter cells after furrow ingression. Anaphase cells possess two distinct populations of microtubules (MTs), generated through either a centrosome-dependent or -independent mechanism. Centrosomal MTs form radial MT arrays called astral MTs, the plus ends of which reach to the cell cortex (Harris, 1961; Inoue and Salmon, 1995). The acentrosomal population of MTs is generated from MT nucleation sites located in the interpolar region and are bundled in an antiparallel manner by the MT-bundling protein PRC1 (Mastronarde *et al.*, 1993; Mollinari *et al.*, 2002; Uehara and Goshima, 2010). Acentrosomal MTs compose the major portion of the bipolar MT bundles, called the central spindle (also called interzonal or midzone MTs; Glotzer, 2009). Both of these MT structures have the capacity to mediate signal transduction for cytokinesis progression by providing scaffolds for major cytokinesis regulators, such as the chromosome passenger complex (CPC) and the centralspindlin complex (Martineau-Thuillier *et al.*, 1998; Adams *et al.*, 2001; Mishima *et al.*, 2002; Murata-Hori and Wang, 2002; Nishimura and Yonemura, 2006). The CPC mediates the phosphoregulation of a wide range of cytokinesis regulators, including components of the centralspindlin (Douglas *et al.*, 2010; Basant *et al.*, 2015; Kitagawa and Lee, 2015), whereas the centralspindlin recruits a Rho-specific guanine exchange factor, ECT2, to the equatorial region (Somers and Saint, 2003; Kamijo *et al.*, 2006; Petronczki *et al.*, 2007; Su *et al.*, 2011). ECT2 then activates the small GTPase RhoA at the equatorial cortex (Tatsumoto *et al.*, 1999; Yuce *et al.*, 2005), which mediates formation of the contractile ring through the activation of effector proteins such as mDia2/Diaphanous (Dean *et al.*, 2005; Watanabe *et al.*, 2008,

This article was published online ahead of print in MBoC in Press (http://www.molbiolcell.org/cgi/doi/10.1091/mbc.E15-02-0101) on January 13, 2016.

†Present address: Division of Molecular Oncology, Institute for Genetic Medicine, Hokkaido University, Sapporo 060-0815, Japan.

*Address correspondence to: Ryota Uehara (ruehara@sci.hokudai.ac.jp).

Abbreviations used: CPC, chromosome passenger complex; EGFP, enhanced green fluorescent protein; FBS, fetal bovine serum; MT, microtubule; PBS, phosphate-buffered saline; PFA, paraformaldehyde; RNAi, RNA interference; siRNA, small interfering RNA.

Supplemental Material can be found at:
http://www.molbiolcell.org/content/suppl/2016/01/11/mbc.E15-02-0101v1.DC1.html

2010), Rho-kinase/Rok/ROCK (Kosako *et al.*, 1999, 2000; Dean and Spudich, 2006; Hickson *et al.*, 2006), and anillin (Hickson and O'Farrell, 2008; Piekny and Glotzer, 2008). As furrow ingression proceeds, MT bundles that pass the equatorial region become tightly packed to form the midbody at the intercellular bridge. At the same time, the centralspindlin becomes concentrated to the central portion of the midbody, where it mediates the connection between the midbody MT bundles and the cellular membrane (Lekomtsev *et al.*, 2012), and recruits factors required for abscission (Zhao *et al.*, 2006; Carlton and Martin-Serrano, 2007; Elia *et al.*, 2011; Guizetti *et al.*, 2011).

The physiological importance of astral MTs and the central spindle in the regulation of cytokinesis has been investigated in a variety of organisms using different experimental approaches, such as microsurgeries that remove or mislocalize these MT structures (Hiramoto, 1956; Rappaport, 1961; Cao and Wang, 1996; Alsop and Zhang, 2003; Bringmann and Hyman, 2005; von Dassow *et al.*, 2009) or gene silencing or mutant analyses of their components (Bonaccorsi *et al.*, 1998; Verbrugghe and White, 2004; Mollinari *et al.*, 2005; Motegi *et al.*, 2006; Bringmann *et al.*, 2007; Werner *et al.*, 2007; Rankin and Wordeman, 2010). These studies suggest that the relative contribution of these MT structures varies among different experimental systems depending on the cell type, shape, or size (Kieserman *et al.*, 2008). A possible interpretation of these results is that anaphase MTs of different origins cooperate in a redundant manner during cytokinesis. On the other hand, a previous study using high-resolution live imaging in monastral anaphase cells suggested that distinct MT populations from different origins have different dynamics and different effects on cortical organization during cytokinesis (Canman *et al.*, 2003). Therefore each population of anaphase MTs that has distinct origins may also play specific roles in cytokinesis regulation.

A simple approach to determine the contribution of distinct MT populations is to selectively inhibit the generation of that population. In this regard, previous studies applied low concentrations of MT-depolymerizing reagents to selectively abolish centrosome-dependent astral MTs and found that astral MTs limit RhoA-mediated cortical contractile activity to a narrow area at the cell equator (Murthy and Wadsworth, 2008; von Dassow *et al.*, 2009). However, no experimental tools are available to specifically perturb the generation of the centrosome-independent MT population.

We previously identified an eight-subunit protein complex, augmin, which recruits the γ-tubulin complex to mitotic spindle MTs and thereby mediates centrosome-independent MT generation within the spindle (Goshima *et al.*, 2008; Lawo *et al.*, 2009; Uehara *et al.*, 2009; Kamasaki *et al.*, 2013). During anaphase, augmin is localized at the chromosome-proximal area in the interchromosomal region and promotes acentrosomal MT generation (Uehara *et al.*, 2009). Depletion of augmin in HeLa cells dramatically suppressed the formation of interpolar acentrosomal MTs without affecting astral MT generation (Uehara and Goshima, 2010). Therefore augmin depletion provides a unique opportunity to explore the role of the acentrosomal population of anaphase MTs in cytokinesis progression.

In the present study, we investigated how cytokinesis is affected when augmin-dependent MTs are reduced in HeLa cells. The loss of augmin-dependent MTs resulted in severe impairment of cleavage furrow ingression. This was caused by the loss of anillin from the equatorial cortex and ectopic formation of astral MT bundles, which impaired efficient pole separation during anaphase. Of interest, the RhoA-activating pathway, which is required for anillin localization, remained intact in augmin-depleted cells. We also found that in the absence of augmin-dependent MTs, the midbody structure was unfocused and detached from the cell cortex, resulting in a high failure rate of cytokinesis completion. These data indicate that postanaphase MTs generated by an augmin-mediated pathway are critical for efficient furrow ingression and completion of cytokinesis.

RESULTS

Cleavage furrow ingression is impaired in augmin-depleted cells

Previously we found that augmin knockdown by RNA interference (RNAi) severely suppressed the formation of central spindle MTs and caused cytokinesis failure in HeLa cells (Uehara *et al.*, 2009). To gain further insight into cytokinesis defects caused by augmin depletion, we depleted the augmin subunit Aug6 (also called FAM29A/HAUS6/hDgt6) with various concentrations of small interfering RNA (siRNA) in enhanced green fluorescent protein (EGFP)–α-tubulin-expressing HeLa cells and observed the progression of cytokinesis using live imaging (Figure 1, A and B; confirmation of protein depletion by immunoblotting is shown in Supplemental Figure S1, A and B). A substantial fraction of these cells showed cleavage furrow regression either during early anaphase, before complete ingression of the cleavage furrow (defined as "early regression"), or in the postfurrowing phase (late regression; Figure 1, A and B, and Supplemental Movie S1). A high frequency of early regression was observed at high concentrations of Aug6 siRNA (Figure 1B). This contrasted with PRC1 depletion, which caused furrow regression mostly after complete ingression of the cleavage furrow, even at high siRNA concentrations (Figure 1, C–E; Mollinari *et al.*, 2005). Quantification of the furrow width at the time of furrow regression revealed that a considerable population of augmin-depleted cells regressed when their furrow width reached ~10 μm, whereas the vast majority of PRC1-depleted cells regressed after their furrow width dropped to <2 μm (Figure 1E and Supplemental Movie S1). We next quantified the time course of furrow ingression and found a considerable delay in augmin-depleted cells compared with control cells (Figure 1, F and G, Supplemental Figure S1, C–E, and Supplemental Movie S2). The maximum furrow ingression rate significantly decreased in an Aug6 siRNA concentration–dependent manner (Figure 1G). The delay in furrow ingression and subsequent furrow regression in Aug6-depleted cells was rescued by expression of an RNAi-resistant version of EGFP-Aug6, ruling out the possibility of RNAi off-target effects (Figure 1, H and I, and Supplemental Figure S1, F and G). Moreover, a delay in furrow ingression was also detected upon depletion of other augmin subunits (Supplemental Figure S1, H and I). In contrast, depletion of PRC1 did not slow down furrow ingression (see later discussion of Figure 5, D and E; Mollinari *et al.*, 2005). These results suggest that augmin-mediated generation of central spindle MTs, but not bundling of central spindle MTs by PRC1, is required for normal progression of the early phase of cytokinesis. Depletion of augmin also caused pleiotropic defects in earlier processes of mitosis, such as centrosome fragmentation and multipolar spindle formation (Supplemental Figure S1, J and K; Einarson *et al.*, 2004; Wu *et al.*, 2008; Lawo *et al.*, 2009). However, in the present study, delayed furrow ingression was observed regardless of the presence or absence of fragmented centrosomes or multipolar spindles (Supplemental Figure S1D).

A delay in furrow ingression was also caused by depletion of a subunit of the γ-tubulin complex NEDD1/GCP-WD (Supplemental Figure S1, L and M), which is required for formation of the central spindle MTs, suggesting that a loss of central spindle MTs, not of augmin per se, affects cleavage furrow ingression in human cells (Uehara and Goshima, 2010).

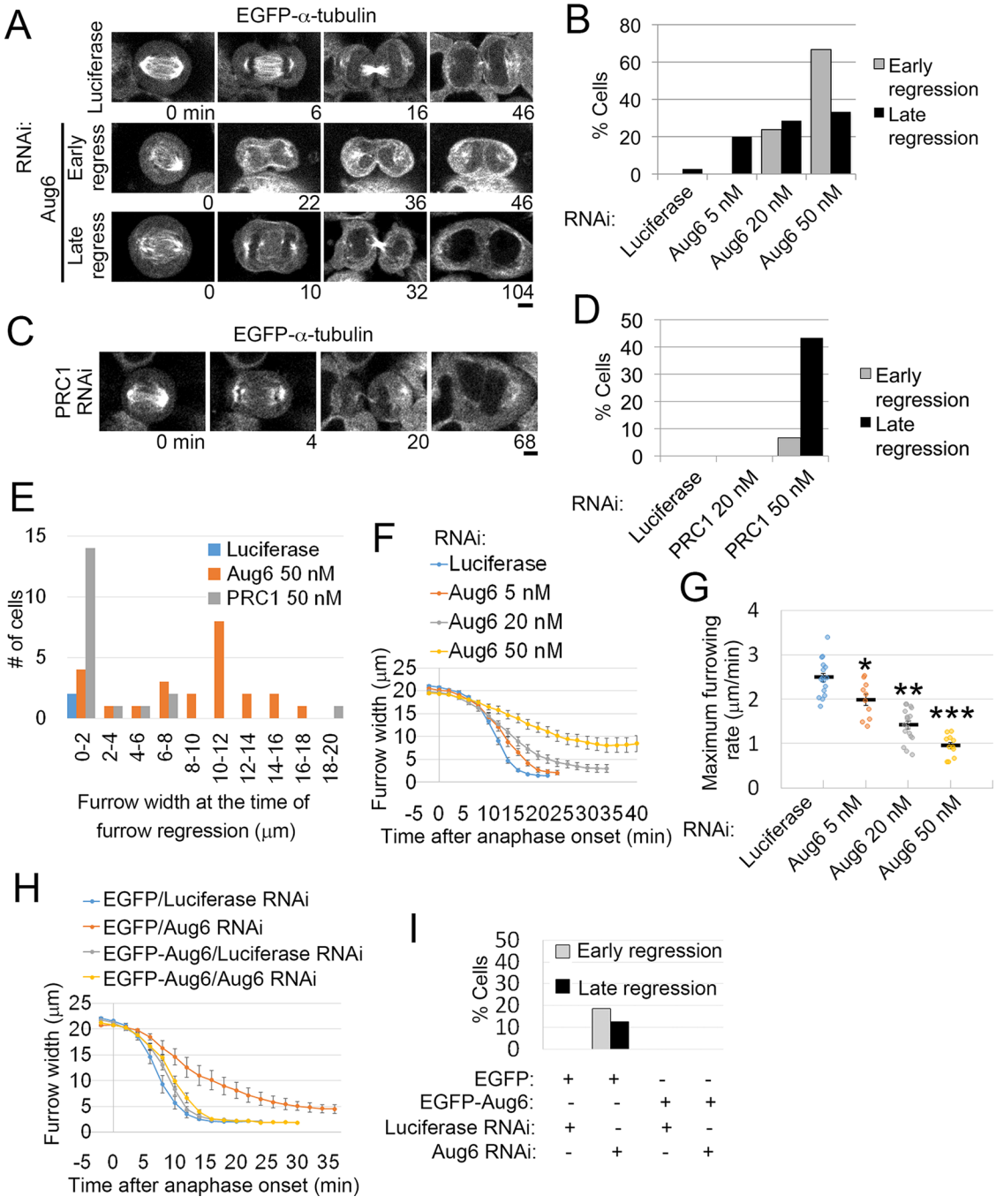

FIGURE 1: Furrowing defects in augmin-depleted cells. (A, C) Time-lapse images of control and Aug6- or PRC1-depleted EGFP–α-tubulin cells. Examples of cells that regressed during furrow ingression (early regression) or after furrow closure (late regression). Time after the onset of anaphase is indicated. Scale bars, 5 μm. (B, D) Frequencies of cytokinesis defects in control and Aug6- or PRC1-depleted cells. At least 12 cells from two independent experiments (B) or ≥30 cells from two independent experiments (D) per condition were analyzed. (E) Furrow widths at the time when the furrow started to regress were quantified in control and Aug6- or PRC1-depleted cells (treated with 50 nM siRNA), and the frequency of the widths is depicted as a histogram. Data were obtained from two independent experiments. Live images were obtained at 2-min time intervals. Examples of live images used for quantification are shown in Supplemental Movie S1. (F, G) Time plot of furrow width change (F) and maximum furrowing rate (G) in EGFP–α-tubulin–expressing cells treated with various concentrations of Aug6 siRNA. Example of an ROI used for quantification is shown in Supplemental Movie S2. Mean ± SE of ≥10 cells from two independent experiments per condition. Depletion of Aug6 significantly decreased furrow ingression (*$p < 0.01$, **$p < 10^{-8}$, ***$p < 10^{-10}$, t test). (H) Time plot of furrow-width change in RNAi-treated cells expressing EGFP or EGFP-Aug6 with RNAi-resistant mutations. Mean ± SE of ≥7 cells from two independent experiments per condition. (I) Frequencies of cytokinesis defects in RNAi-treated cells expressing EGFP or EGFP-Aug6 with RNAi-resistant mutations. At least 16 cells from two independent experiments per condition were analyzed.

Cytokinesis regulators accumulate at the equatorial region of dividing cells via ectopically formed astral MT bundles in the absence of the central spindle

We next investigated the effect of augmin depletion on signal transduction of the cytokinesis regulatory pathway by testing the organization of MTs and the localization of MT-associated key cytokinesis regulators—the antiparallel MT-bundling protein PRC1, the centralspindlin complex (using RacGAP1 as a marker), ECT2, and the CPC (using Aurora B as a marker). In control cells, these proteins were localized to the midzone of the central spindle, as previously reported (Nislow *et al.*, 1992; Jiang *et al.*, 1998; Martineau-Thuillier *et al.*, 1998; Tatsumoto *et al.*, 1999; Giet and Glover, 2001; Mishima *et al.*, 2002; Figure 2, A–D). However, in augmin-depleted cells, the formation of the central spindle was severely impaired, and RacGAP1, PRC1, and Aurora B were substantially less abundant within the central area of the equatorial plane. At the same time, the amount of MTs, RacGAP1, ECT2, and PRC1 was significantly increased in the proximity of the equatorial cell cortex (Figure 2, A–J). These peripheral MTs originated from the centrosomes at opposite spindle poles and appeared to be linked in the equatorial area, where PRC1 and RacGAP1 were also localized (Supplemental Figure S2, A and B). PRC1 and augmin codepletion substantially diminished peripheral MTs, as well as RacGAP1 and ECT2 localization to these MTs (Figure 2, A, D, F, and I). In contrast, the localization of Aurora B to the cortex-proximal region was unaffected by augmin or PRC1 depletion (Figure 2, C and H). It is possible that Aurora B is recruited to the equatorial cortex via astral MTs, as previously suggested (Murata-Hori and Wang, 2002). These results indicate that, in the absence of augmin-dependent MTs, astral MTs are bundled in an antiparallel manner by PRC1, which in turn provides scaffolds for the ectopic accumulation of centralspindlin and ECT2 at the equatorial cortex proximal region.

Reduction of anillin at the equatorial cortex causes defects in furrow ingression in augmin-depleted cells

We next tested the effect of augmin depletion on contractile ring formation by assessing the localization of key regulators and components of the contractile ring during furrow ingression. RhoA was localized to the equatorial cortex at a similar level in augmin-depleted cells compared with control cells (Figure 3, A, E and F, and Supplemental Figure S3, A–D). The distribution of RhoA along the cell cortex was also unchanged upon augmin depletion (Figure 3G). Localization of the RhoA effector protein citron kinase (Madaule *et al.*, 1998) at the equatorial cortex also remained unaffected in augmin-depleted cells (Supplemental Figure S3, A and B). Because RhoA activation is required for accumulation of both RhoA itself and citron kinase to the equatorial cortex (Kamijo *et al.*, 2006; Nishimura and Yonemura, 2006), these results, combined with the fact that RhoA regulators were recruited to the equatorial region via the ectopically formed astral MT bundles (Figure 2), suggest that activation of RhoA occurs at the cleavage furrow in the absence of augmin-dependent MTs. Consistent with this interpretation, the main components of the contractile ring, myosin II and F-actin, whose accumulation at the contractile ring is also RhoA dependent (Yuce *et al.*, 2005; Kamijo *et al.*, 2006), were localized to the cleavage furrow at similar levels in augmin-depleted cells compared with control cells (Figure 3, B, C, and E–G, and Supplemental Figure S3E). Surprisingly, however, the accumulation of anillin at the cleavage furrow was significantly reduced in augmin-depleted cells (Figure 3, D–G, and Supplemental Figure S3, F–H), whereas cytoplasmic levels of anillin were unchanged (Supplemental Figure S3, I and J). The anillin localization at the cleavage furrow decreased as concentrations of Aug6 siRNA increased, whereas localization of myosin II in the same cells was unchanged (Supplemental Figure S3, K–M). Costaining for RhoA and anillin confirmed that localization of anillin to the cleavage furrow was attenuated in augmin-depleted cells in the presence of normal amounts of RhoA at the cleavage furrow (Supplemental Figure S3,C and D). Therefore, even though the RhoA-dependent pathway remained intact in augmin-depleted cells, the accumulation of anillin to the cleavage furrow was specifically impaired. Despite the substantial reduction of anillin at the equatorial cortex in augmin-depleted cells, the frequency of abnormal oscillatory contraction of the cell cortex, which is observed in anillin-depleted cells (Straight *et al.*, 2005; Hickson and O'Farrell, 2008; Piekny and Glotzer, 2008), remained at a normal level (one of 16 control cells) with a wide range of Aug6 siRNA concentrations (one of 10 cells, 0 of 18 cells, or one of 11 cells treated with 5, 20, or 50 nM Aug6 siRNA, respectively). The reason for the absence of oscillatory contraction in augmin-depleted cells is unclear, but one possible explanation is that abnormal configuration of the anaphase MT structure in these cells may suppress the polar cortical contraction that drives oscillatory motion.

Next we tested whether anillin overexpression was able to compensate for the depletion of augmin. In augmin-depleted cells, the exogenous expression of anillin-EGFP restored anillin recruitment to the equatorial cortex at levels similar to those of control mock-depleted EGFP–α-tubulin–expressing cells (Figure 4, A and B). The efficiency of augmin RNAi was unchanged (Supplemental Figure S4A). Of interest, anillin-EGFP expression significantly suppressed the delay in furrow ingression (Figure 4, C and D, and Supplemental Figure S4D) and substantially reduced the incidence of early cleavage furrow regression (Figure 4E). Expression of EGFP-myosin IIA, which presumably reinforces the contractility of the contractile ring, also partially rescued the furrow ingression defect observed in augmin-depleted cells (Supplemental Figure S4, B, E, and F). These were not general effects of EGFP-tagged protein expression, as the expression of other tagged proteins, such as EGFP-mDia2 or Cep55-EGFP, was not able to rescue these defects (Supplemental Figure S4, A, C, and G–J). We conclude that augmin is required for efficient cleavage furrow ingression due in part to its function in targeting anillin to the equatorial cortex. Our results suggest that augmin-dependent MTs are required for the formation of a functional contractile ring that supports the furrowing process.

We next tested whether the reduction of anillin at the cleavage furrow was sufficient to cause the early cytokinesis defects observed in augmin-depleted cells. The partial depletion of anillin using a low siRNA concentration, resulting in levels similar to those in augmin-depleted cells (Supplemental Figure S5, A and B), frequently caused abnormal oscillatory contraction of the cell cortex during furrow ingression (Supplemental Figure S5, C and D; Straight *et al.*, 2005; Hickson and O'Farrell, 2008; Piekny and Glotzer, 2008). This resulted in regression of the partially ingressed furrow. However, anillin depletion had much less effect on the kinetics of furrow ingression than did augmin depletion (Supplemental Figure S5, E and F). Therefore the reduction of anillin at the equatorial cortex alone cannot explain the severe delay in furrow ingression in augmin-depleted cells.

Ectopic astral MT bundles impede spindle pole separation, chromosome segregation, and efficient furrow ingression in augmin-depleted cells

To explore additional factors that affect furrow ingression, we compared the kinetics of spindle pole separation in control and augmin-depleted cells expressing EGFP–α-tubulin. During anaphase in control cells, spindle poles separate from each other with a stalling

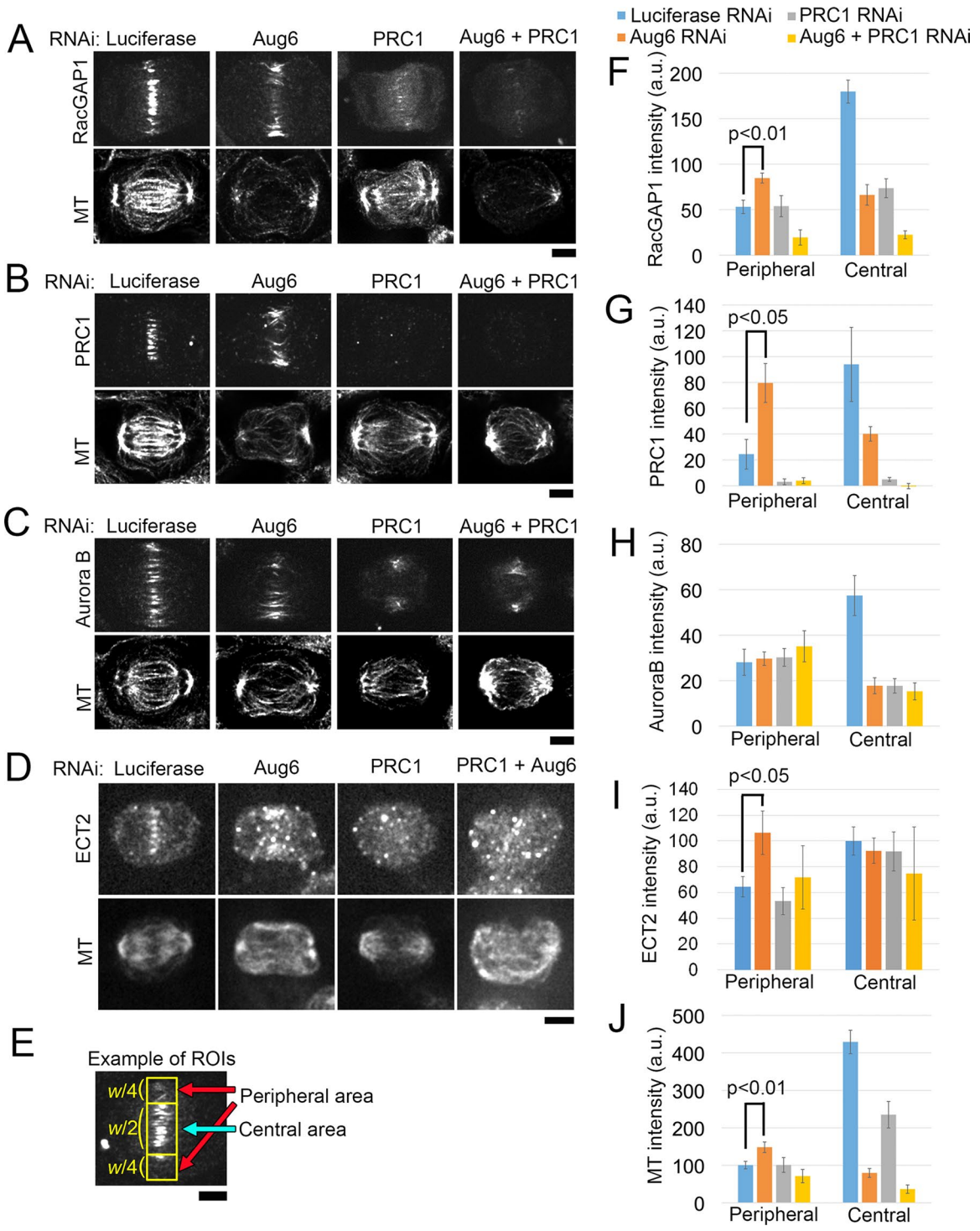

FIGURE 2: Cytokinesis regulators are recruited to the cell equator via astral MT bundles in the absence of a central spindle. (A–D) Immunostaining for RacGAP1 (A), PRC1 (B), Aurora B (C), ECT2 (D), and MTs in RNAi-treated anaphase cells. (E) Example of an ROI used for quantification in F–J (yellow boxes). *w*, width of the equatorial region. Only cells in the early phase of furrow ingression were chosen for analysis (see *Materials and Methods* for details). (F–J) Quantification of immunostaining intensity of RacGAP1 (F), PRC1 (G), Aurora B (H), ECT2 (I), and MTs (J) in the central or peripheral area of the equatorial regions in RNAi-treated cells. Mean ± SE of ≥5 cells (F), ≥4 cells (G), ≥6 cells (H), ≥3 cells (I), and ≥15 cells (J) from two independent experiments per condition. The signal intensities of RacGAP1, PRC1, ECT2, and MTs were significantly increased in the peripheral area after depletion of Aug6 (*p* value from the *t* test). Whereas the ECT2 signal at the central spindle diminished in Aug6-depleted cells, the immunostaining intensity at the central area remained at the control level, presumably because of high background. Scale bars, 5 μm.

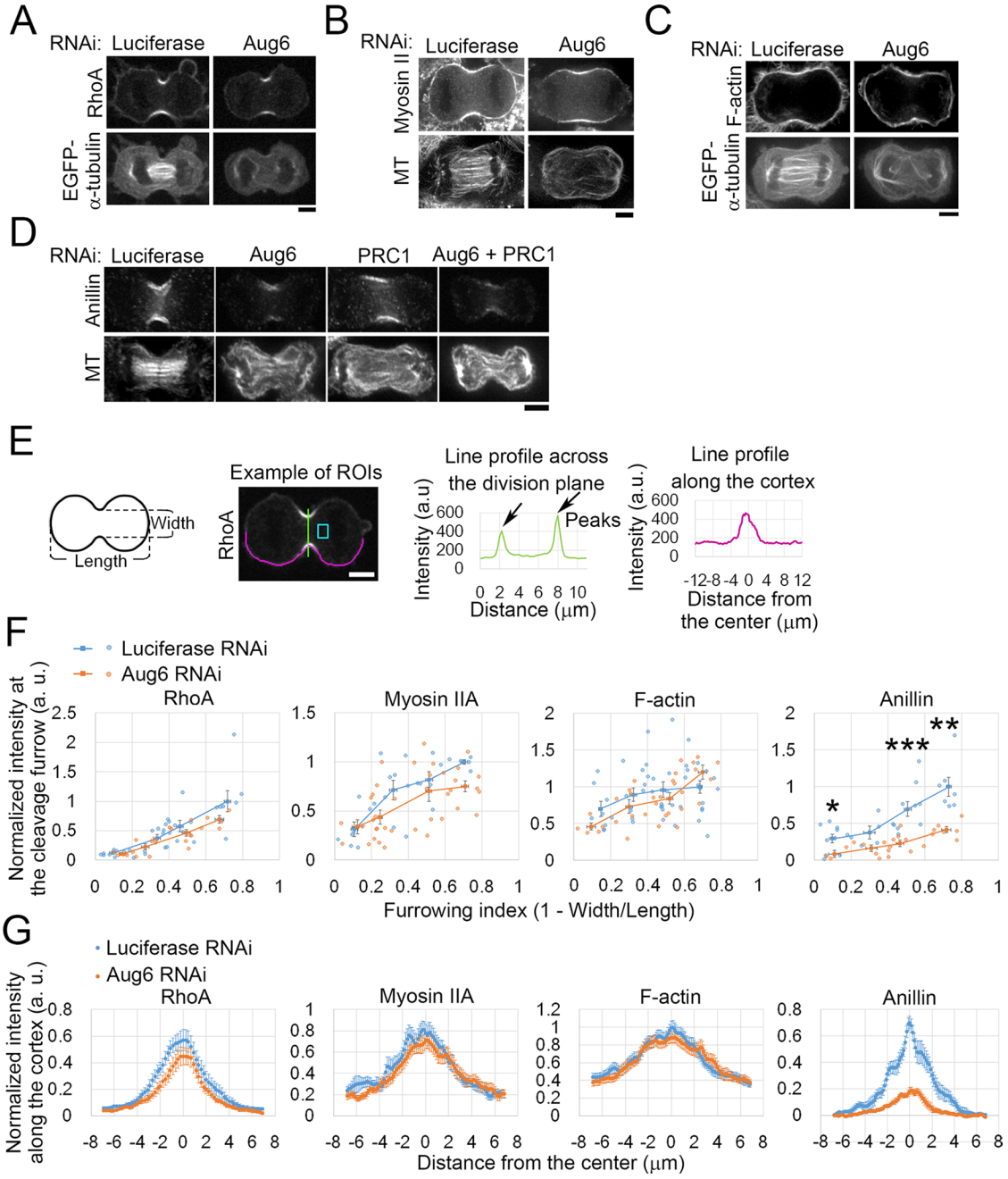

FIGURE 3: Defects in formation of the contractile ring in augmin-depleted cells. (A–D) Immunostaining for RhoA (A), myosin IIA heavy chain (B), and anillin (D) or staining of F-actin by rhodamine-phalloidin (C) in RNAi-treated cells. MTs were visualized by either immunostaining (B, D) or EGFP–α-tubulin (A, C). (E) Left, for quantification in F and G, the dividing cells were categorized based on the progression of furrow ingression, which was quantified using a furrowing index, defined as (1 – furrow width/cell length). See *Materials and Methods* for details. Middle and right, example of an ROI used for quantification in F (a line profile across the division plane, green) and G (a line profile along the cortex, magenta). The light blue box indicates the cytoplasmic region used for background subtraction. (F) Normalized intensity of RhoA, myosin IIA, F-actin, or anillin staining at the cleavage furrow during the progression of furrowing. Each data point corresponds to the average of two peak intensities of a line profile (E) from each single cell. Data points were binned at a 0.2 interval of the furrowing index, and the mean ± SE of the bins is shown as squares with a line. Data were normalized to the mean intensity of controls at the bin of the furrowing index 0.6–0.8. At least 24 cells (RhoA), ≥28 cells (myosin IIA), ≥32 cells (F-actin), or ≥24 cells (anillin) from at least two independent experiments per condition were analyzed. Depletion of Aug6 significantly decreased anillin accumulation at the cleavage furrow (*$p < 0.05$, **$p < 0.01$, ***$p < 0.001$; *t* test). (G) Normalized intensities of RhoA, myosin IIA, F-actin, and anillin along the cell cortex. Data from the cells with a furrowing index of 0.4–0.6 (corresponding to the furrowing phase). Two line profiles were derived from both sides of each single cell. Mean ± SE of ≥8 cells (RhoA), ≥6 cells (myosin IIA), ≥13 cells (F-actin), or ≥9 cells (anillin) from at least two independent experiments per condition. Scale bars, 5 μm.

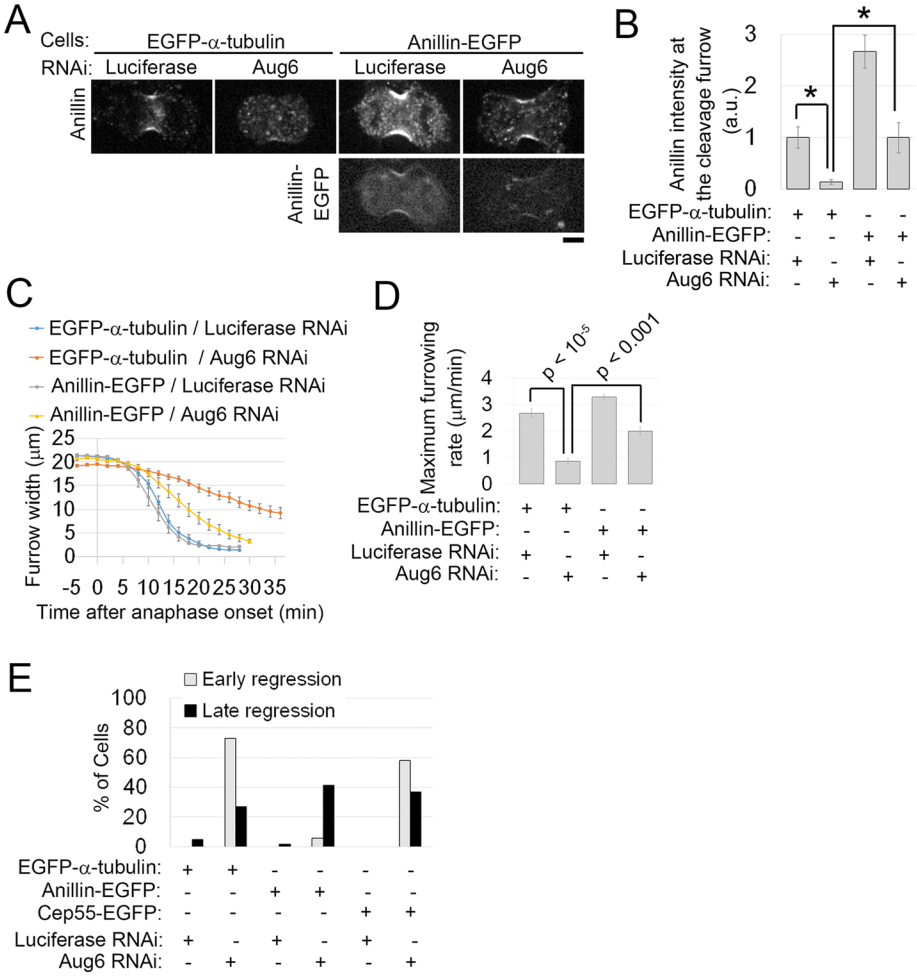

FIGURE 4: Exogenous expression of EGFP-anillin rescues early cytokinesis defects in Aug6-depleted cells. (A) Immunostaining for anillin in RNAi-treated cells expressing EGFP–α-tubulin or anillin-EGFP. Scale bar, 5 μm. (B) Normalized intensity of anillin staining at the cleavage furrow. Mean ± SE of ≥5 cells from two independent experiments per condition. Asterisks indicate statistically significant differences ($p < 0.05$, *t* test). An example of the ROIs used for quantification is shown in Supplemental Figure S3G. (C, D) Time plot of furrow-width change (C) and maximum furrowing rate (D) in RNAi-treated EGFP–α-tubulin– or anillin-EGFP–expressing cells. Mean ± SE of ≥6 cells from two independent experiments per condition. *p* values from *t* tests. (E) Frequencies of cytokinesis defects in control or Aug6-depleted cells. At least 17 cells from four independent experiments per condition were analyzed. In anillin-EGFP–expressing cells, the early regression induced by Aug6 depletion was dramatically rescued, whereas it was not rescued in other control cells (EGFP–α-tubulin– or Cep55-EGFP–expressing cells).

phase corresponding to anaphase A, followed by a rapid separation phase corresponding to anaphase B (Figure 5, A and B). In augmin-depleted cells, the pole-to-pole distance of the preanaphase spindle was slightly longer than in control cells (Figure 5, A and B). However, after anaphase onset, spindle pole separation was delayed by a longer stalling phase, resulting in a significantly shorter pole-to-pole distance during furrow ingression (Figure 5, B and C). Because incomplete spindle pole separation impedes furrow ingression in early nematode and sea urchin embryos (Dechant and Glotzer, 2003; von Dassow *et al.*, 2009), we next tested whether the restoration of pole separation was able to rescue the furrow ingression defect in augmin-depleted cells. Unbundling of central spindle MTs through reduced expression of PRC1 accelerates spindle pole separation during anaphase in amphibian embryonic cells (Kieserman *et al.*, 2008). We therefore reasoned that resolution of the ectopic astral MT bundles by codepletion of PRC1 with augmin would accelerate spindle pole separation in augmin-depleted cells. Indeed, codepletion of PRC1 partially restored the rates of pole separation and furrow ingression (Figure 5, A, B, D, and E, and Supplemental Figure S6, A–E). Of importance, codepletion of PRC1 and augmin did not restore anillin levels at the equatorial cortex to normal (Figure 3D and Supplemental Figure S3H). Given these results, it is possible that the astral MT bundles that form ectopically in augmin-depleted cells slow spindle pole separation during anaphase and generate an inhibitory effect on furrow ingression independent of anillin recruitment. In augmin-depleted cells, we also occasionally observed missegregated chromosomes (Supplemental Figure S3, K and M). However, the frequency of furrow ingression delay was much higher than that of chromosome missegregation (Figure 1, F and G, and Supplemental Figures S1C and S3M). It is therefore unlikely that chromosome missegregation is the primary cause of the furrow ingression defects that we observed. On the basis of these results, we suggest that the pole separation defect, combined with the delocalization of anillin from the equatorial cortex, causes severe furrow ingression failure in augmin-depleted cells.

Augmin function is required for the symmetrical distribution of cytokinesis regulators around the cell equator

Besides the delay in furrow ingression, we found that furrow ingression became highly asymmetrical in a substantial population of augmin-depleted cells, with furrow invagination occurring predominantly on one side of the cell (e.g., 3 of 9 cells treated with 50 nM Aug6 siRNA; Figure 6, A–D). The frequency of asymmetrical furrow ingression increased with higher concentrations of Aug6 siRNA (Figure 6, C and D). Given that the occurrence of asymmetrical furrow ingression in augmin-depleted cells did not correlate with the severity of the ingression delay (Supplemental Figure S1E), these furrowing defects could be caused by an independent mechanism. We observed that in augmin-depleted cells centralspindlin (marked by MKLP1) and RhoA were recruited more toward one side of the furrow (Figure 6, E–G). Therefore, although augmin-dependent MTs were not required for recruiting a sufficient level of signaling molecules for contractile ring formation (Figures 2 and 3), they were required for uniform distribution of these signaling molecules to ensure symmetrical furrow ingression.

Augmin-mediated MTs are required for the concentration of midbody components

Live-cell imaging revealed that even when augmin-depleted cells completed furrow ingression, many of them subsequently regressed their cleavage furrow within a 0- to 40-min time frame (Uehara *et al.*, 2009; Figure 1A and Supplemental Figure S7, A–D).

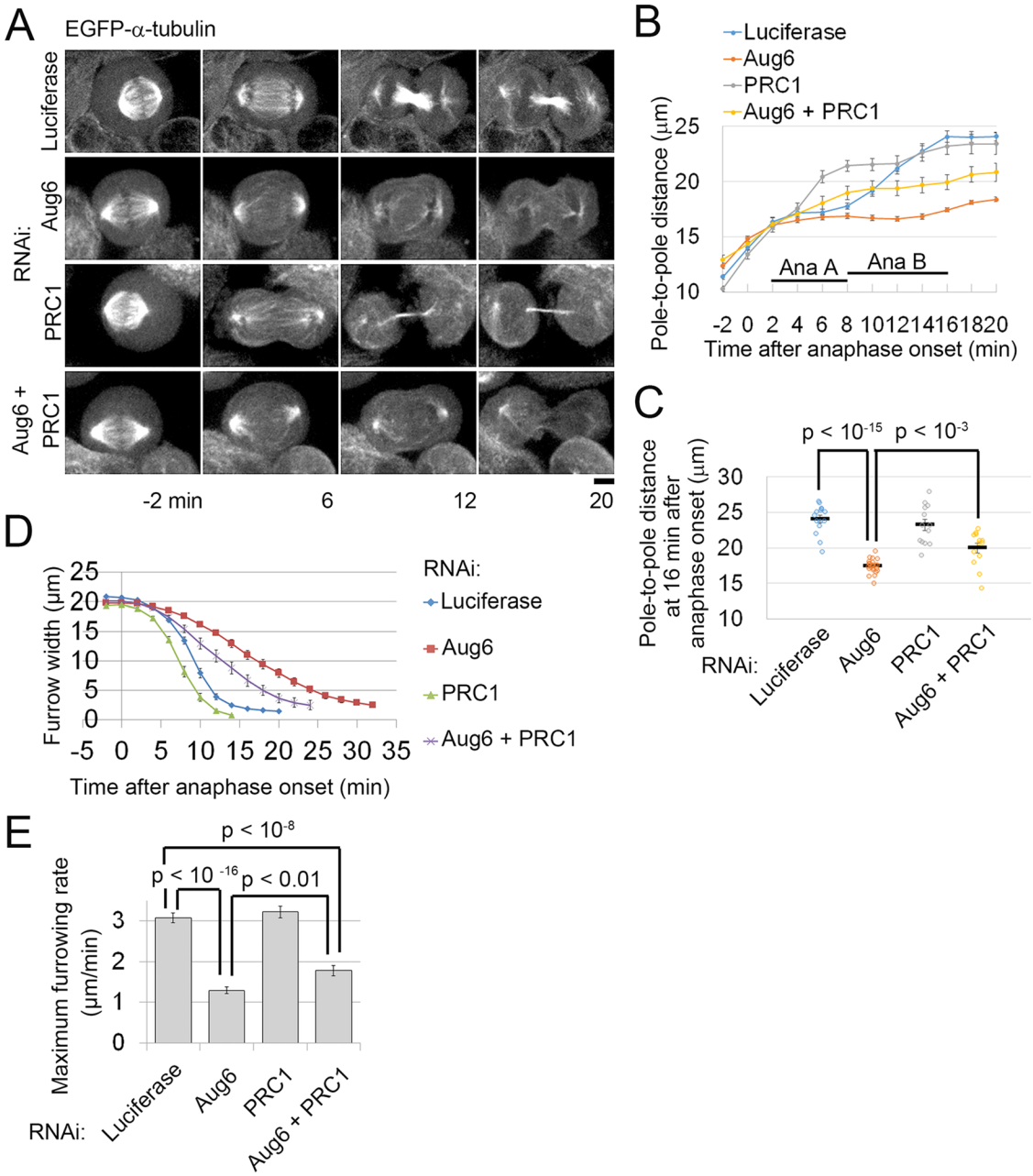

FIGURE 5: Codepletion of PRC1 with Aug6 partially rescues defects in spindle pole separation and furrow ingression in augmin-depleted cells. (A) Time-lapse images of RNAi-treated EGFP–α-tubulin cells. Time after the onset of anaphase is indicated. Scale bar, 5 μm. (B, C) Time plot (B) and raw data points (at 16 min after anaphase onset; C) of pole-to-pole distance in RNAi-treated, EGFP–α-tubulin cells. Mean ± SE of ≥13 cells from two independent experiments per condition (*p* values from the *t* test). (D, E) Time plot of furrow- width change (D) and maximum furrowing rate (E) in RNAi-treated EGFP–α-tubulin cells. Mean ± SE of ≥ 20 cells from three independent experiments per condition (*p* values from the *t* test).

This suggests that the loss of augmin-dependent MTs affects progression of the postfurrowing stages of cytokinesis, as well as furrow ingression. We found that anillin levels at the intercellular bridge were reduced in augmin-depleted cells (Supplemental Figure S7, E and F). However, the expression of anillin-EGFP did not rescue the late regression caused by augmin depletion (Figure 4E). Furthermore, the partial depletion of anillin, which delocalized anillin from the equatorial cortex to levels similar to those found in augmin-depleted cells, did not lead to late cleavage furrow regression (Supplemental Figures S5D and S7, G and H). This suggests that, in addition to anillin, other factors that are required for abscission depend on augmin function.

To investigate the late cytokinesis defects caused by augmin depletion, we imaged live cells expressing EGFP–α-tubulin or RacGAP1-EGFP. As furrow ingression proceeded, peripheral MT bundles labeled with EGFP–α-tubulin or RacGAP1-EGFP became compressed into dense bundles to form the intercellular MT bridge (Figure 7A and Supplemental Figure S7I). Immunostaining revealed that these peripheral MT bundles accumulated cytokinesis regulators, such as PRC1, RacGAP1, MKLP1, and Aurora B, at the intercellular bridge

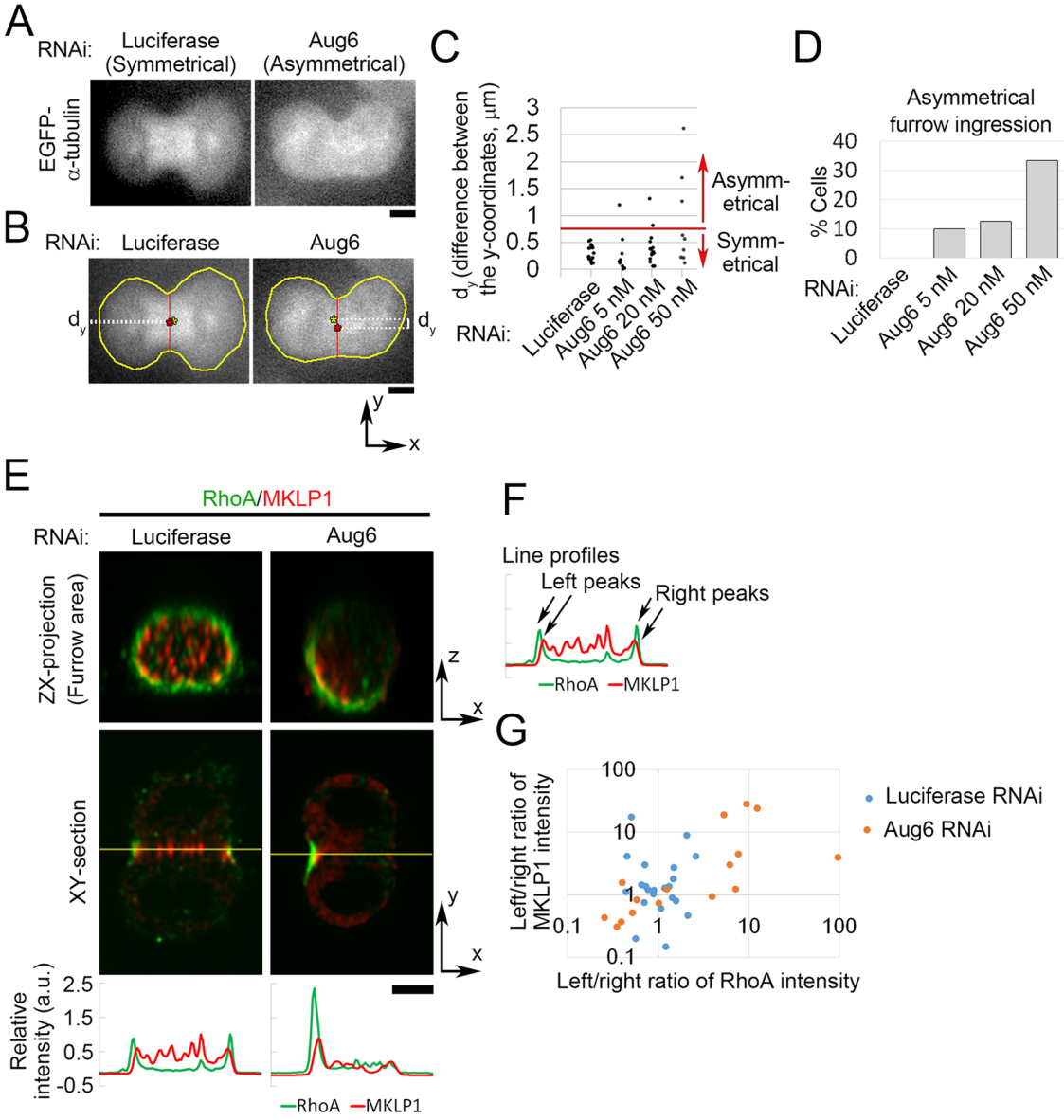

FIGURE 6: Asymmetrical furrow ingression frequently occurs in augmin-depleted cells. (A) Example of asymmetrical furrow ingression in Aug6-depleted EGFP–α-tubulin cells. (B) To quantify the symmetry of furrow ingression, images of dividing cells were rotated to set their division axes horizontally, and d_y, the difference between the *y*-coordinates of the centroid of the whole cell (yellow asterisk) and the midpoint of the line connecting both edges of the furrow (red asterisk), was measured. A frame of sequential live images at which the furrow passed 60% of the initial width of the cell equator was chosen for quantification. (C) Quantification of d_y in EGFP–α-tubulin cells treated with various concentrations of Aug6 siRNA. The threshold was set at 7.5, such that cells with a d_y value greater than this were defined as asymmetrical. (D) Frequencies of asymmetrical furrow ingression in cells treated with various concentrations of Aug6 RNAi. At least nine cells from two experiments per condition were analyzed in C and D. (E) Orthogonal views of an RNAi-treated cell immunostained with anti-MKLP1 and anti-RhoA antibodies. Line profiles of immunostaining intensity along the line across the division plane (yellow lines). (F, G) To quantify the symmetry of MKLP1 and RhoA distribution in control and Aug6-depleted cells, left/right ratios of peak intensities in the line profiles (F) are plotted in G. The ratios deviated further from 1 in Aug6-depleted cells than in controls. At least 16 cells from two experiments per condition were analyzed. Scale bars, 5 μm.

(Figure 7B). This was reminiscent of central spindle MTs that form in normal cells; however, the midzone components were more broadly distributed and diffuse than with control cells (Figure 7B). In augmin-depleted cells, RacGAP1 levels at the center of the intercellular bridge were reduced to 46% that of control levels ($n \geq 12$; Figure 7C), showing that the broader distribution of centralspindlin was accompanied by a substantial reduction in its local concentration at the intercellular bridge.

The disorganization of the intercellular bridge in augmin-depleted cells could be an indirect effect of delayed furrow ingression. To test the effect of augmin depletion on centralspindlin distribution independently of furrow ingression, we used MG132 to arrest control and augmin-depleted RacGAP1-EGFP cells at metaphase and then treated them with the Plk1 inhibitor BI-2536 in the presence of MG132 (Figure 7, D–F, and Supplemental Figure S7J). Within the time window of our observations (40 min after BI-2356 treatment),

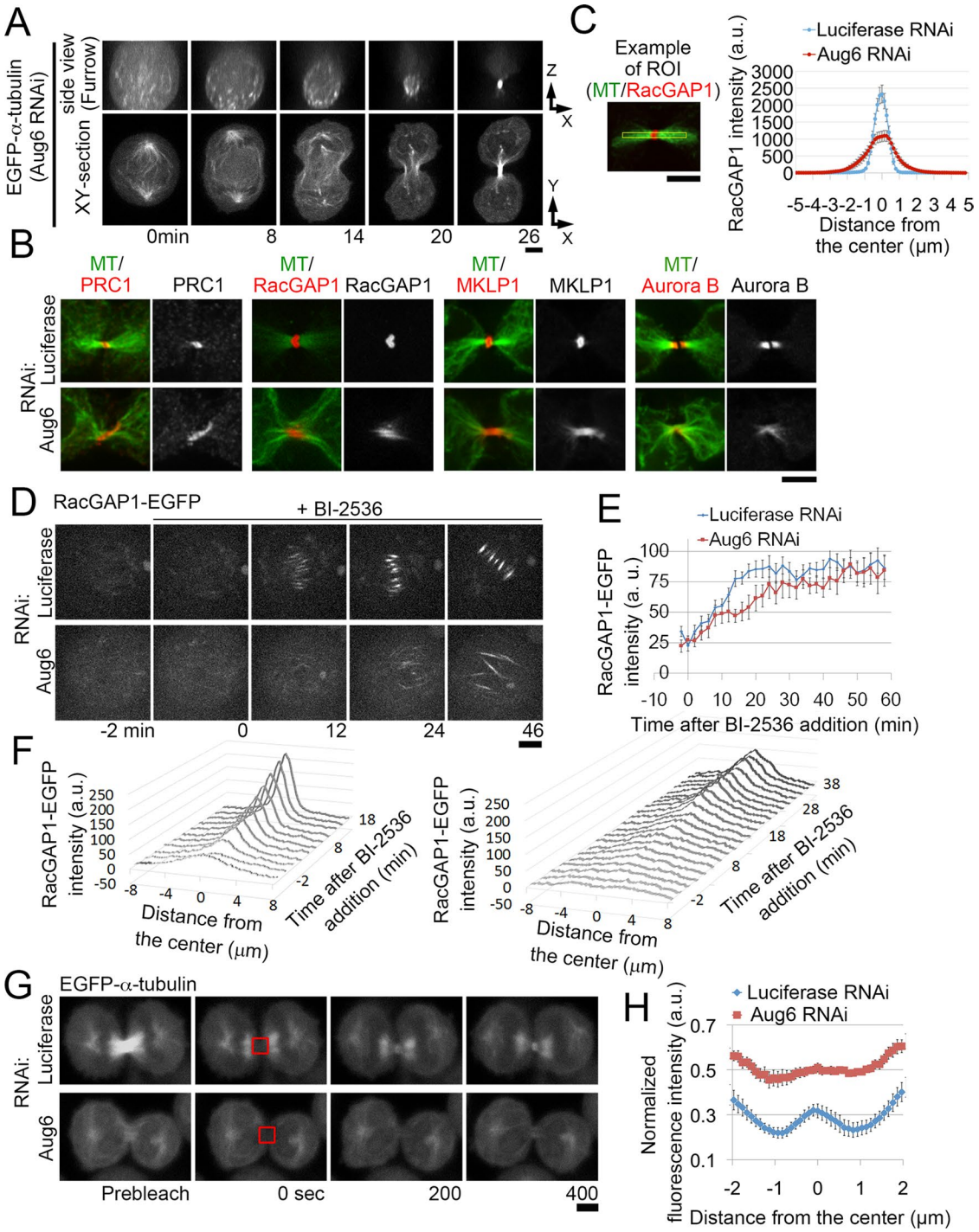

FIGURE 7: Broadening of the spindle midzone in augmin-depleted cells. (A) Orthogonal views of an Aug6-depleted, EGFP–α-tubulin cell. (B) Immunostaining for cytokinesis regulators and MTs at the intercellular bridge of RNAi-treated cells. (C) Line profiles of RacGAP1 immunostaining intensity along the division axes in control and Aug6-depleted cells. Mean ± SE of ≥12 cells from two independent experiments per condition. The signal intensity at the center of the intercellular bridge was significantly reduced in Aug6-depleted cells ($p < 0.001$, t test). An example of the ROIs used for the quantification is shown on the left. (D) Time-lapse images of control and Aug6-depleted RacGAP1-EGFP cells treated with BI2536 during metaphase. The time before and after addition of the drug is indicated. (E) Time plot of RacGAP1-EGFP intensity on the spindle in BI2536-treated metaphase cells in D. Mean ± SE of ≥10 cells from two independent experiments per condition. (F) Line profiles of RacGAP1-EGFP intensity along the spindle axes in D. Mean of ≥10 cells from two independent experiments per condition. An example of the ROIs is shown in Supplemental Figure S7J. (G) Fluorescence recovery after photobleaching at the intercellular bridge (red boxes) in RNAi-treated EGFP–α-tubulin cells. (H) Line profiles of recovered fluorescence along the intercellular bridge in G. Fluorescence intensity at each position at 400 s after photobleaching was normalized to that before photobleaching. Mean ± SE of ≥8 cells from two independent experiments per condition. Examples of ROIs are shown in Supplemental Figure S7L. Scale bars, 5 μm.

all of the drug-treated cells stayed in prometaphase or metaphase with unsegregated chromosomes (shown by propidium iodide staining of the chromosomes; 24 of 24 control cells and 45 of 45 augmin-depleted cells; Supplemental Movie S3). It was reported that this treatment blocks Plk1-dependent inhibitory PRC1 phosphorylation and induces formation of premature central spindle–like MT bundles (Hu *et al.*, 2012). Reportedly, however, these MT bundles lack some authentic central spindle components, such as ECT2, presumably because of the inhibitory effect of Plk1 suppression on their recruitment mediated by RacGAP1 (Burkard *et al.*, 2009; Wolfe *et al.*, 2009), and fail to induce cleavage furrow formation (Hu *et al.*, 2012). In control cells, RacGAP1-EGFP was sparsely distributed over a broad area of the spindle before treatment, but within 20 min after BI-2536 treatment, it became dramatically concentrated at the center of the MT bundles, forming spindle midzone–like structures (Figure 7, D–F, and Supplemental Figure S7J). In augmin-depleted cells, RacGAP1-EGFP accumulated more slowly over a substantially broader area of the MT bundles than with controls (Figure 7, D–F). The depletion of NEDD1 also broadened the range of RacGAP1-EGFP localization (Supplemental Figure S7K). These results suggest that a specific population of MTs generated by augmin and γ-tubulin complexes is required for proper localization of centralspindlin to a defined area of antiparallel MT bundles, independently of furrow ingression control.

To gain further insight into the spatial distribution of MTs at the intercellular bridge after augmin depletion, we photobleached the intercellular bridge region in EGFP–α-tubulin cells and analyzed the spatial patterns of fluorescence recovery in the bleached area (Figure 7, G and H, and Supplemental Figure S7L). In unperturbed mammalian somatic cells, MT plus ends localize predominately to the spindle midzone (Mastronarde *et al.*, 1993; Elad *et al.*, 2011; Guizetti *et al.*, 2011). We therefore expected to see the highest fluorescence recovery in this region because of the polymerization/depolymerization dynamics of the MT plus ends. Indeed, in control cells, fluorescence recovery occurred predominantly at the center of the intercellular bridge (Figure 7, G and H). In augmin-depleted cells, however, fluorescence recovery occurred over a substantially broader region, suggesting that the dynamic MT plus ends are distributed throughout the intercellular bridge (Figure 7, G and H). These results suggest that after augmin depletion, MTs are not organized into well-focused interdigitated MT arrays, which may explain why the midbody components fail to concentrate within the narrow midbody area at the intercellular bridge.

Peripheral MT bundles fail to mediate MT–membrane interactions at the intercellular bridge

Next we investigated how midbody disorganization in augmin-depleted cells affects the late stages of cytokinesis by imaging CHMP4B-EGFP, a component of the abscission machinery, and its upstream targeting factor, Cep55-EGFP (Guizetti and Gerlich, 2010; Elia *et al.*, 2013). In control cells, Cep55-EGFP started to accumulate at the midzone of the central spindle during furrow ingression and continued to accumulate monotonically to the center of the intercellular bridge (Supplemental Figure S7, A and B). In contrast, CHMP4B-EGFP accumulated only at the midzone, ~40 min after complete furrow ingression (Supplemental Figure S7, C and D; Elia *et al.*, 2011; Guizetti *et al.*, 2011). In augmin-depleted cells, initial accumulation of Cep55-EGFP at the intercellular bridge appeared normal, but it did not reach peak levels, and most cells showed cleavage furrow regression (Supplemental Figure S7, A and B). CHMP4B-EGFP accumulation was never detected in augmin-depleted cells with cleavage furrow regression (Supplemental Figure S7, C and D), suggesting that the intercellular bridge, which is derived from peripheral MT bundles, fails to maintain cleavage furrow ingression until the abscission machinery is assembled.

We next imaged the intercellular bridge of augmin-depleted cells using transmission electron microscopy (TEM). Consistent with the immunostaining results described here earlier, the midbody matrix, an electron-dense material at the intercellular bridge (Mierzwa and Gerlich, 2014), was less focused and more dispersed along the division axis in augmin-depleted cells (Figure 8; five of five cells). Furthermore, the plasma membrane appeared detached from the midbody (Figure 8 and Supplemental Figure S7M; three of five cells. Given that centralspindlin has been reported to mediate the MT–membrane connection during cytokinesis (Lekomtsev *et al.*, 2012), the dilution of centralspindlin at the center of the intercellular bridge in augmin-depleted cells (Figure 7C) might attenuate the integrity of the bridge structure. To test this possibility, we monitored the progression of cytokinesis in cells partially depleted of MKLP1, where levels of centralspindlin at the center of the intercellular bridge were similar to those in augmin-depleted cells (Supplemental Figure S7, N–P). These treatments substantially increased the frequency of late regression (Supplemental Figure S7P), supporting the idea that the dilution of centralspindlin on the MT bundles underlies the cleavage furrow regression phenotype.

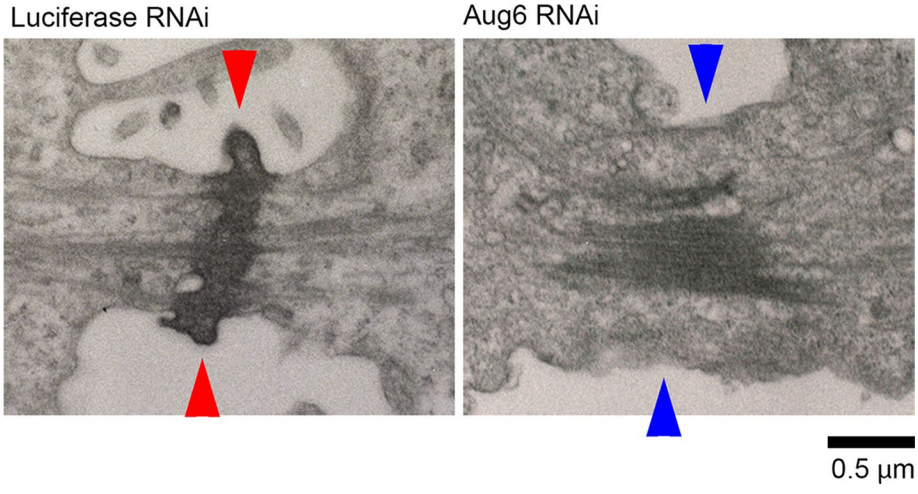

FIGURE 8: Destabilization of the intercellular bridge in augmin-depleted cells. TEM images of the intercellular bridge in RNAi-treated cells. In control cells, the connection between midbody and cell membrane was established (red arrowheads), whereas it was severely impaired in Aug6-depleted cells (blue arrowheads). Scale bar, 0.5 μm.

DISCUSSION

Importance of augmin-dependent MTs in regulating efficient cleavage furrow ingression

In this study, we extensively analyzed the progression of cytokinesis after specifically suppressing the generation of augmin-dependent MTs in HeLa cells. We observed a defect in furrow ingression in augmin-depleted cells. This defect is likely to be general consequence of the loss of the acentrosomal interpolar MTs, since the depletion of NEDD1, another factor required for the generation of these MTs, caused a similar

furrowing defect. Because depletion of PRC1, an interpolar MT bundling protein, did not prevent furrow ingression (Mollinari *et al.*, 2005), these MTs do not necessarily have to be in a bundled state to fulfill their role in controlling furrow ingression. Of importance, astral MTs remained functional but failed to support efficient furrow ingression in augmin-depleted cells. Our data therefore indicate the nonredundant contribution of a specific MT population generated by augmin to the regulation of early cytokinesis progression.

We found that anillin recruitment to the equatorial cortex is severely impaired in augmin-depleted cells. Of importance, the RhoA activation pathway remained intact through astral MT–mediated recruitment of cytokinesis regulators to the equatorial cortex in these cells. Previous studies showed that RhoA inhibition abolishes the accumulation of anillin at the equatorial cortex (Hickson and O'Farrell, 2008; Piekny and Glotzer, 2008). Our results therefore suggest that both augmin-dependent MTs and active RhoA are required for the localization of anillin. One possible augmin-dependent anillin targeting mechanism could be a direct interaction between augmin-dependent MTs and the equatorial cortex. A previous study reported that a subpopulation of interchromosomal MTs elongate and contact the equatorial cortex in mammalian somatic cells (Canman *et al.*, 2003), and the direct interaction between anaphase MTs and cortical anillin has also been shown in cultured cells from *Drosophila* (Hickson and O'Farrell, 2008). Alternatively, it is possible that augmin-dependent MTs transmit signals to the distal cortex through a molecular diffusion–based mechanism to induce contractile ring formation, as proposed in echinoderm embryos (von Dassow *et al.*, 2009). Another possibility is that augmin-dependent MTs control the availability of free anillin required for contractile ring formation by limiting the growth of astral MTs, which were shown to sequester anillin from the equatorial cortex (van Oostende Triplet *et al.*, 2014). In the absence of augmin-dependent MT generation, the excess pool of free tubulin may get incorporated into centrosome-dependent MTs, leading to an overgrowth of astral MTs. This could, in turn, lead to the depletion of free anillin available for contractile ring formation. Our finding that complementing the anillin pool by exogenous expression of anillin-EGFP restored the net accumulation of anillin at the equatorial cortex in augmin-depleted cells supports this idea (Figure 4, A and B). These mechanisms are not mutually exclusive, and it will be interesting to investigate the dynamics of anillin accumulation at the equatorial cortex in the presence or absence of augmin-dependent MTs in future studies.

In augmin-depleted cells, efficient spindle pole separation during anaphase was inhibited probably through the formation of the ectopic astral MT bundles, which may provide friction and oppose pole movement. A decrease in the interpolar distance during anaphase would result in an increase in the local density of astral MTs at the equatorial cortex, which may in turn suppress the contractile activity of the cortex, as proposed and observed in other systems (Yoshigaki, 1999; Dechant and Glotzer, 2003; Werner *et al.*, 2007; Murthy and Wadsworth, 2008; von Dassow *et al.*, 2009). Because either an increase in anillin at the furrow or the resolution of ectopic astral MT bundles formation by codepletion of PRC1 with augmin alone can rescue the substantial reduction in the rates of furrow ingression in augmin-depleted cells, these two defects may synergistically cause the severe furrowing defects. A similar synergistic effect between loss of the central spindle and failure in spindle pole separation on the progression of cytokinesis has been reported in early nematode and sea urchin embryos (Dechant and Glotzer, 2003; von Dassow *et al.*, 2009). We propose that augmin-dependent MT generation secures efficient furrow ingression both by controlling the accumulation of anillin at the equatorial cortex and keeping spindle poles, which generate an inhibitory effect on furrow ingression, away from the cell equator.

Augmin-dependent MTs are required for the formation of a functional spindle midzone

During the late stages of cytokinesis, we found that the depletion of augmin resulted in a dramatic loss of the interaction between MTs and the cell membrane at the intercellular bridge. It is unlikely that augmin directly mediates membrane–MT anchoring, since augmin is localized at both distal ends of the central spindle, not at the center of the structure (Uehara *et al.*, 2009) where the MTs and membrane are connected. A more likely explanation for this phenotype is the abnormal distribution and reduction of centralspindlin at the intercellular bridge, which has been reported to mediate the MT–membrane connection (Lekomtsev *et al.*, 2012). Previous studies reported that broadening of the midzone, either through introduction of a motor-dead mutant of CHO1/MKLP1 or depletion of Kif4a, caused late cleavage furrow regression (Matuliene and Kuriyama, 2002; Kurasawa *et al.*, 2004; Hu *et al.*, 2011). We therefore conclude that the augmin-mediated assembly of the central spindle MTs is important for the formation of a focused spindle midzone structure at the intercellular bridge that supports persistent MT–membrane anchoring and abscission. We do not understand the mechanism by which the midbody components become unfocused in the absence of augmin. One possible explanation is that a substantial reduction in the net amount of MT at the intercellular bridge by augmin depletion may reduce scaffolds for accumulation of these components, resulting in their mislocalization. Another possibility is that disorganization of minus ends of anaphase MTs through delocalization of the γ-tubulin complex by augmin depletion could alter the organization of the whole MT structure within the midbody, including its central region, as previously reported in cells depleted of the minus end–directed motor, HSET (Cai *et al.*, 2010). Ultrastructural analyses of the disorganized intercellular bridge at the single MT level in augmin-depleted cells would be informative to distinguish between these two possibilities.

MATERIALS AND METHODS

Cell culture and DNA transfection

The HeLa-Kyoto line, HeLa BAC cell lines expressing RacGAP1-LAP (Hutchins *et al.*, 2010), anillin-LAP (Uehara *et al.*, 2013), Cep55-LAP, or CHMP4B-LAP and the HeLa EGFP–α-tubulin line (Steigemann *et al.*, 2009) were cultured in DMEM supplemented with 10% fetal bovine serum (FBS) and 1× antibiotic-antimycotic (Sigma-Aldrich, St. Louis, MO). DNA transfection was performed using JetPEI (Polyplus-transfection, Illkirch, France). HeLa-Kyoto EGFP-Aug6 and EGFP-myosin IIA lines were established by transfecting HeLa Kyoto cells with pEGFP-Aug6 or pEGFP-myosin IIA vector, respectively, and selecting positive cells in the presence of 500 µg/ml G418. For the experiments in Supplemental Figure S4, C, G, and H, HeLa Kyoto cells transiently transfected with the pEGFP-mDia2 vector were used. For live-cell imaging, cells were cultured in phenol red–free DMEM supplemented with 10% FBS and 1× antibiotic-antimycotic.

Plasmids

The plasmid encoding a RNAi-resistant version of EGFP-Aug6 (pEGFP-C1-Aug6) has been described previously (Uehara *et al.*, 2009). pEGFP-C3-myosin IIA for expression of EGFP-myosin IIA (Wei and Adelstein, 2000) was purchased from Addgene (plasmid #11347). Full-length cDNA of human mDia2 (GenBank accession

no. NM_001042517.1) was obtained from the RPE1 cell cDNA pool by PCR using primers 5′-ATCTCGAGCTATGGAACGGCACCAGC-CGCGGCTGC-3′ and 5′-ATGGTACCTTATAAAGCTCGTAATCTT-GCCAGC-3′ and subcloned into the *Xho*I–*Kpn*I sites of pEGFP-C1 (Takara Bio, Kusatsu, Japan).

RNAi

siRNA transfection was performed using Lipofectamine RNAiMAX (Invitrogen, Carlsbad, CA). To inhibit the function of augmin, we depleted Aug6 or Aug1, either of which is an essential subunit of the protein complex (Uehara *et al.*, 2009). The siRNAs used in this study were 5′-CAGUUAAGCAGGUACGAAATT-3′ (Aug6) (Uehara *et al.*, 2009), 5′-GCGAGAACUAGAUAGCAUUTT-3′ (Aug1) (Uehara *et al.*, 2009), 5′-AAAUAUGGGAGCUAAUUGGGA-3′ (PRC1#1), 5′-CAUUUAUGGUGAAUGGGCATT-3′ (PRC1#2), 5′-CGAUGCC-UCUUUGAAUAAATT-3′ (anillin) (Piekny and Glotzer, 2008), 5′-GCAGACAUGUGUCAAUUUATT-3′ (NEDD1) (Luders *et al.*, 2006), 5′-AAGCAGUCUUCCAGGUCAUCUUU-3′ (MKLP1) (Douglas *et al.*, 2010), and 5′-CGUACGCGGAAUACUUCGATT-3′ (luciferase). Cells were observed 2 d after siRNA treatment in all experiments, except for Supplemental Figures S5, A–F, S7, G, H, and N–P, for which they were observed 1 d after treatment.

Antibodies

Mouse monoclonal anti-RacGAP1 antibody, rabbit anti-Aug6, and anti-Aug8 antisera were reported previously (Goshima *et al.*, 2008; Uehara and Goshima, 2010; Uehara *et al.*, 2013). The mouse monoclonal anti-MKLP1 antibody was obtained using the keyhole limpet hemocyanin–conjugated peptide (CTPRFGSKSKSATNLGRQGN) as an antigen and following the previously described procedure (Kimura *et al.*, 1994). Rabbit anti-Aug1 antiserum was obtained by cloning full-length Aug1 to pDEST17 (Invitrogen), purifying the bacterially expressed protein, and subjecting it to rabbit immunization. Rabbit anti-myosin heavy chain antiserum was a gift from K. Owaribe (Nagoya University, Nagoya, Japan; Masuda *et al.*, 1984). Specificity of the anti–myosin heavy chain antiserum against the HeLa cell extract was confirmed by immunoblotting (Supplemental Figure S3E). Rat monoclonal anti–α-tubulin antibody (YOL1/34; AbD Serotec, Raleigh, NC), mouse monoclonal anti-aurora B antibody (611082; BD Biosciences, Franklin Lakes, NJ), rabbit monoclonal anti-PRC1 antibody (ab51248; Abcam, Cambridge, United Kingdom), goat polyclonal anti-PRC1 antibodies (sc-9342; Santa Cruz Biotechnology, Dallas, TX), mouse monoclonal anti-NEDD1 antibody (H00121441-M05; Abnova, Taipei, Taiwan), goat polyclonal anti-anillin antibodies (sc-54859; Santa Cruz Biotechnology), rabbit polyclonal anti-ECT2 antibody (sc-1005; Santa Cruz Biotechnology), goat polyclonal anti–citron kinase (sc-1848; Santa Cruz Biotechnology), mouse monoclonal anti-RhoA antibody (sc-418; Santa Cruz Biotechnology), and rat monoclonal anti-GFP (GF090R; Nacalai Tesque, Kyoto, Japan) were purchased from suppliers as indicated.

Immunoblotting

For immunoblotting, the RNAi-treated cells were lysed in 1× SDS–PAGE sample buffer, boiled for 3 min, and subjected to SDS–PAGE, using 5–20% gradient acrylamide gels. The immunoblotting was performed using an anti-Aug6 antiserum (1:500), an anti-Aug8 antiserum (1:500), an anti-Aug1 antiserum (1:100), an anti-anillin antiserum (1:200), an anti–Aurora B antibody (1:200), an anti-MKLP1 antibody (1:10), an anti-NEDD1 antibody (1:100), anti-PRC1 antibodies (1:250), an anti–α-tubulin antibody (1:1000), an anti–myosin heavy chain antiserum (1:1000), an anti-GFP antibody (1:1000), and horseradish peroxidase–conjugated anti-rabbit, anti-rat, or anti-mouse antibodies (1:1000) at the indicated dilutions. For signal detection, the Clarity Western ECL Substrate (Bio-Rad, Hercules, CA) and an ImageQuant LAS 4000 mini-imager (GE Healthcare, Pittsburgh, PA) were used.

Immunostaining

For all of the immunostaining experiments except those in Figures 2D, 3A, 4A, and 6E and Supplemental Figure S3, A and C, the cells were fixed with 3.2% paraformaldehyde (PFA) in phosphate-buffered saline (PBS) for 10 min and then permeabilized with 0.5% Triton X-100 in PBS for 10 min at 25°C. Because we found that the PFA fixation restricted the access of anti-anillin antibodies to the exogenously expressed anillin-EGFP protein at the cleavage furrow, we fixed the cells with 100% methanol at −20°C for 10 min for the experiment shown in Figure 4A. In addition, immunostaining for ECT2 in Figure 2D was performed using methanol fixation. For immunostaining of RhoA in Figures 3A and 6E and Supplemental Figure S3, A and C, the cells were fixed with prechilled 10% trichloroacetic acid on ice for 15 min (Nishimura and Yonemura, 2006), followed by permeabilization with 0.2% Triton X-100 in PBS supplemented with 0.1 M glycine for 5 min at room temperature. For the F-actin staining shown in Figure 3C, the cells were prefixed with 1% glutaraldehyde in PBS, postfixed with 4% PFA in PBS, permeabilized with 0.5% Triton X-100 in PBS for 10 min, and then treated with 20 mM $NaBH_4$ for 30 min at room temperature. The fixed cells were incubated with the primary antibodies overnight at 4°C, washed three times with PBS, and incubated with the secondary antibodies for 1 h at room temperature. For immunostaining, the antibodies were used at a dilution of 1:2 (anti-MKLP1 antibody), 1:10 (anti-RacGAP1 antibody), 1:100 (anti-ECT2 antibody, anti-RhoA antibody, and anti–citron kinase antiserum), 1:400 (anti-PRC1 antibodies and anti–Aurora B antibody), 1:500 (anti-anillin antibodies), or 1:1000 (anti–α-tubulin antibody, anti–myosin heavy chain antiserum, and fluorescence dye–conjugated secondary antibodies). To stain chromosomes or F-actin, 4′,6-diamidino-2-phenylindole (Dojindo, Kamimashiki, Japan), propidium iodide (Dojindo), or Acti-stain 555 phalloidin (Cytoskeleton, Denver, CO) was used at a final concentration of 1.0 μg/ml, 10 μg/ml, or 100 nM, respectively. The immunostained samples were washed three times with PBS and mounted with Fluoromount (Diagnostic BioSystems, Pleasanton, CA).

Cell imaging

The fixed and living cells were observed under a TE2000 microscope (Nikon, Tokyo, Japan) equipped with a 100×/1.4 numerical aperture (NA) Plan-Apochromatic, a 60×/1.4 NA Plan-Apochromatic, or a 40×/1.3 NA Plan Fluor oil immersion objective lens (Nikon), a CSU-X1 confocal unit (Yokogawa, Tokyo, Japan), and an iXon3 electron-multiplier charge coupled device camera (Andor, Belfast, United Kingdom). Image acquisition was controlled by μManager software. Fluorescence recovery after photobleaching was performed using a C2 (Nikon) confocal microscope equipped with a 60×/1.4 NA oil immersion objective lens (Nikon). TEM was performed as previously described (Uehara *et al.*, 2013).

Induction of a premature midzone structure in metaphase cells

The induction of premature central spindle–like MT bundles in metaphase cells was performed as previously described (Hu *et al.*, 2012), with slight modifications. RNAi-treated RacGAP1-EGFP cells were incubated with 10 μM MG132 for ~2 h and then with 125 nM BI-2536 and 10 μM MG132 at 37°C and then subjected to either live-cell imaging or fixation.

Image analyses

Quantification of the fluorescence intensities by microscopy was performed using ImageJ software (National Institutes of Health, Bethesda, MD). To standardize the progression of furrow ingression in fixed postanaphase cell samples, we used a furrowing index, defined as 1 − furrow width/cell length (Figure 3E; Uehara and Goshima, 2010). This index changes from 0 to 1 as a round-shaped cell cleaves into two daughter cells. For the quantification shown in Figure 2, cells with a furrowing index ranging from 0 to 0.4 (in early anaphase) were chosen, and the mean fluorescence intensities at the peripheral or central areas of the cell equator (depicted in Figure 2E) were subtracted by those of the cytoplasmic areas outside the cell equator. For the quantification in Figure 4B and Supplemental Figures S3H and S5B, cells with a furrowing index from 0.3 to 0.9 (in furrowing phase) were chosen, and the mean fluorescence intensities at the equatorial cortex (depicted in Supplemental Figure S3G) were subtracted by those of the cytoplasmic areas outside the cell equator. For the quantification of the time-course fluctuations of the GFP intensities shown in Figure 7E and Supplemental Figure S7, B and D, the mean fluorescence intensities in manually selected spindle midzone regions (depicted in Supplemental Figure S7B) were subtracted by those in the cytoplasmic areas (for Figure 7E) or the areas outside the cells (for Supplemental Figure S7, B and D) and then multiplied by the areas of the midzone regions to obtain total fluorescence intensities. The intensity at each time point was normalized to the fluorescence intensity of the whole cell at the initial time point in order to normalize the difference in expression levels of the EGFP-tagged proteins. For the line profiles, the fluorescence intensities in Figure 7, C, F, and H, were taken using the plot profile command within the ImageJ software (regions of interest [ROIs] are shown in Figure 7C and Supplemental Figure S7, J and L). For the quantification in Supplemental Figure S7, F and H, the mean fluorescence intensities at the center of the intercellular bridge (ROIs of area 2.4 μm × 2.4 μm) in postfurrowing cells were subtracted by those of the areas outside the cells. The three-dimensional (3D) reconstructed images of the dividing cells shown in Figures 6E and 7A and Supplemental Figure S7I were obtained using the 3D projection command within the ImageJ software.

ACKNOWLEDGMENTS

We are grateful to Naohito Nozaki (Mab Institute, Sapporo, Japan), Katsushi Owaribe and Jiro Usukura (Nagoya University, Nagoya, Japan), and Tony Hyman (Max Planck Institute, Dresden, Germany) for providing antibodies, offering assistance with transmission electron microscopy, and providing cell lines, respectively. This work was supported by the Akiyama Life Science Foundation, the Mochida Memorial Foundation, the Naito Foundation, the Nakajima Foundation, the Northern Advancement Center for Science and Technology, the SGH Foundation, and the Sumitomo Foundation (to R.U.), the Takeda Science Foundation and the Uehara Memorial Foundation (to R.U. and G.G.), Japan Ministry of Education, Culture, Sports, Science, and Technology Grants-in-Aid for Scientific Research (to R.U., J.Y., and G.G.), the Seventh Framework Programme FP7/2007-2013 under Grant Agreements 241548 (MitoSys; to I.P. and D.W.G.) and 258068 (Systems Microscopy), and an ERC Starting Grant (Agreement 281198; to D.W.G.).

REFERENCES

Adams RR, Maiato H, Earnshaw WC, Carmena M (2001). Essential roles of Drosophila inner centromere protein (INCENP) and aurora B in histone H3 phosphorylation, metaphase chromosome alignment, kinetochore disjunction, and chromosome segregation. J Cell Biol 153, 865–880.

Alsop GB, Zhang D (2003). Microtubules are the only structural constituent of the spindle apparatus required for induction of cell cleavage. J Cell Biol 162, 383–390.

Basant A, Lekomtsev S, Tse YC, Zhang D, Longhini KM, Petronczki M, Glotzer M (2015). Aurora B kinase promotes cytokinesis by inducing centralspindlin oligomers that associate with the plasma membrane. Dev Cell 33, 204–215.

Bonaccorsi S, Giansanti MG, Gatti M (1998). Spindle self-organization and cytokinesis during male meiosis in asterless mutants of Drosophila melanogaster. J Cell Biol 142, 751–761.

Bringmann H, Cowan CR, Kong J, Hyman AA (2007). LET-99, GOA-1/GPA-16, and GPR-1/2 are required for aster-positioned cytokinesis. Curr Biol 17, 185–191.

Bringmann H, Hyman AA (2005). A cytokinesis furrow is positioned by two consecutive signals. Nature 436, 731–734.

Burkard ME, Maciejowski J, Rodriguez-Bravo V, Repka M, Lowery DM, Clauser KR, Zhang C, Shokat KM, Carr SA, Yaffe MB, Jallepalli PV (2009). Plk1 self-organization and priming phosphorylation of HsCYK-4 at the spindle midzone regulate the onset of division in human cells. PLoS Biol 7, e1000111.

Cai S, Weaver LN, Ems-McClung SC, Walczak CE (2010). Proper organization of microtubule minus ends is needed for midzone stability and cytokinesis. Curr Biol 20, 880–885.

Canman JC, Cameron LA, Maddox PS, Straight A, Tirnauer JS, Mitchison TJ, Fang G, Kapoor TM, Salmon ED (2003). Determining the position of the cell division plane. Nature 424, 1074–1078.

Cao LG, Wang YL (1996). Signals from the spindle midzone are required for the stimulation of cytokinesis in cultured epithelial cells. Mol Biol Cell 7, 225–232.

Carlton JG, Martin-Serrano J (2007). Parallels between cytokinesis and retroviral budding: a role for the ESCRT machinery. Science 316, 1908–1912.

Dean SO, Rogers SL, Stuurman N, Vale RD, Spudich JA (2005). Distinct pathways control recruitment and maintenance of myosin II at the cleavage furrow during cytokinesis. Proc Natl Acad Sci USA 102, 13473–13478.

Dean SO, Spudich JA (2006). Rho kinase's role in myosin recruitment to the equatorial cortex of mitotic Drosophila S2 cells is for myosin regulatory light chain phosphorylation. PLoS One 1, e131.

Dechant R, Glotzer M (2003). Centrosome separation and central spindle assembly act in redundant pathways that regulate microtubule density and trigger cleavage furrow formation. Dev Cell 4, 333–344.

Douglas ME, Davies T, Joseph N, Mishima M (2010). Aurora B and 14–3-3 coordinately regulate clustering of centralspindlin during cytokinesis. Curr Biol 20, 927–933.

Einarson MB, Cukierman E, Compton DA, Golemis EA (2004). Human enhancer of invasion-cluster, a coiled-coil protein required for passage through mitosis. Mol Cell Biol 24, 3957–3971.

Elad N, Abramovitch S, Sabanay H, Medalia O (2011). Microtubule organization in the final stages of cytokinesis as revealed by cryo-electron tomography. J Cell Sci 124, 207–215.

Elia N, Ott C, Lippincott-Schwartz J (2013). Incisive imaging and computation for cellular mysteries: lessons from abscission. Cell 155, 1220–1231.

Elia N, Sougrat R, Spurlin TA, Hurley JH, Lippincott-Schwartz J (2011). Dynamics of endosomal sorting complex required for transport (ESCRT) machinery during cytokinesis and its role in abscission. Proc Natl Acad Sci USA 108, 4846–4851.

Giet R, Glover DM (2001). Drosophila aurora B kinase is required for histone H3 phosphorylation and condensin recruitment during chromosome condensation and to organize the central spindle during cytokinesis. J Cell Biol 152, 669–682.

Glotzer M (2009). The 3Ms of central spindle assembly: microtubules, motors and MAPs. Nat Rev Mol Cell Biol 10, 9–20.

Goshima G, Mayer M, Zhang N, Stuurman N, Vale RD (2008). Augmin: a protein complex required for centrosome-independent microtubule generation within the spindle. J Cell Biol 181, 421–429.

Guizetti J, Gerlich DW (2010). Cytokinetic abscission in animal cells. Semin Cell Dev Biol 21, 909–916.

Guizetti J, Schermelleh L, Mantler J, Maar S, Poser I, Leonhardt H, Muller-Reichert T, Gerlich DW (2011). Cortical constriction during abscission involves helices of ESCRT-III-dependent filaments. Science 331, 1616–1620.

Harris P (1961). Electron microscope study of mitosis in sea urchin blastomeres. J Biophys Biochem Cytol 11, 419–431.

Hickson GR, Echard A, O'Farrell PH (2006). Rho-kinase controls cell shape changes during cytokinesis. Curr Biol 16, 359–370.
Hickson GR, O'Farrell PH (2008). Rho-dependent control of anillin behavior during cytokinesis. J Cell Biol 180, 285–294.
Hiramoto Y (1956). Cell division without mitotic apparatus in sea urchin eggs. Exp Cell Res 11, 630–636.
Hu CK, Coughlin M, Field CM, Mitchison TJ (2011). KIF4 regulates midzone length during cytokinesis. Curr Biol 21, 815–824.
Hu CK, Ozlu N, Coughlin M, Steen JJ, Mitchison TJ (2012). Plk1 negatively regulates PRC1 to prevent premature midzone formation before cytokinesis. Mol Biol Cell 23, 2702–2711.
Hutchins JR, Toyoda Y, Hegemann B, Poser I, Heriche JK, Sykora MM, Augsburg M, Hudecz O, Buschhorn BA, Bulkescher J, *et al*. (2010). Systematic analysis of human protein complexes identifies chromosome segregation proteins. Science 328, 593–599.
Inoue S, Salmon ED (1995). Force generation by microtubule assembly/disassembly in mitosis and related movements. Mol Biol Cell 6, 1619–1640.
Jiang W, Jimenez G, Wells NJ, Hope TJ, Wahl GM, Hunter T, Fukunaga R (1998). PRC1: a human mitotic spindle-associated CDK substrate protein required for cytokinesis. Mol Cell 2, 877–885.
Kamasaki T, O'Toole E, Kita S, Osumi M, Usukura J, McIntosh JR, Goshima G (2013). Augmin-dependent microtubule nucleation at microtubule walls in the spindle. J Cell Biol 202, 25–33.
Kamijo K, Ohara N, Abe M, Uchimura T, Hosoya H, Lee JS, Miki T (2006). Dissecting the role of Rho-mediated signaling in contractile ring formation. Mol Biol Cell 17, 43–55.
Kieserman EK, Glotzer M, Wallingford JB (2008). Developmental regulation of central spindle assembly and cytokinesis during vertebrate embryogenesis. Curr Biol 18, 116–123.
Kimura K, Nozaki N, Saijo M, Kikuchi A, Ui M, Enomoto T (1994). Identification of the nature of modification that causes the shift of DNA topoisomerase II beta to apparent higher molecular weight forms in the M phase. J Biol Chem 269, 24523–24526.
Kitagawa M, Lee SH (2015). The chromosomal passenger complex (CPC) as a key orchestrator of orderly mitotic exit and cytokinesis. Front Cell Dev Biol 3, 14.
Kosako H, Goto H, Yanagida M, Matsuzawa K, Fujita M, Tomono Y, Okigaki T, Odai H, Kaibuchi K, Inagaki M (1999). Specific accumulation of Rho-associated kinase at the cleavage furrow during cytokinesis: cleavage furrow-specific phosphorylation of intermediate filaments. Oncogene 18, 2783–2788.
Kosako H, Yoshida T, Matsumura F, Ishizaki T, Narumiya S, Inagaki M (2000). Rho-kinase/ROCK is involved in cytokinesis through the phosphorylation of myosin light chain and not ezrin/radixin/moesin proteins at the cleavage furrow. Oncogene 19, 6059–6064.
Kurasawa Y, Earnshaw WC, Mochizuki Y, Dohmae N, Todokoro K (2004). Essential roles of KIF4 and its binding partner PRC1 in organized central spindle midzone formation. EMBO J 23, 3237–3248.
Lawo S, Bashkurov M, Mullin M, Ferreria MG, Kittler R, Habermann B, Tagliaferro A, Poser I, Hutchins JR, Hegemann B, *et al*. (2009). HAUS, the 8-subunit human Augmin complex, regulates centrosome and spindle integrity. Curr Biol 19, 816–826.
Lekomtsev S, Su KC, Pye VE, Blight K, Sundaramoorthy S, Takaki T, Collinson LM, Cherepanov P, Divecha N, Petronczki M (2012). Centralspindlin links the mitotic spindle to the plasma membrane during cytokinesis. Nature 492, 276–279.
Luders J, Patel UK, Stearns T (2006). GCP-WD is a gamma-tubulin targeting factor required for centrosomal and chromatin-mediated microtubule nucleation. Nat Cell Biol 8, 137–147.
Madaule P, Eda M, Watanabe N, Fujisawa K, Matsuoka T, Bito H, Ishizaki T, Narumiya S (1998). Role of citron kinase as a target of the small GTPase Rho in cytokinesis. Nature 394, 491–494.
Martineau-Thuillier S, Andreassen PR, Margolis RL (1998). Colocalization of TD-60 and INCENP throughout G2 and mitosis: evidence for their possible interaction in signalling cytokinesis. Chromosoma 107, 461–470.
Mastronarde DN, McDonald KL, Ding R, McIntosh JR (1993). Interpolar spindle microtubules in PTK cells. J Cell Biol 123, 1475–1489.
Masuda H, Owaribe K, Hayashi H, Hatano S (1984). Ca2+-dependent contraction of human lung fibroblasts treated with Triton X-100: a role of Ca2+-calmodulin-dependent phosphorylation of myosin 20,000-dalton light chain. Cell Motil 4, 315–331.
Matuliene J, Kuriyama R (2002). Kinesin-like protein CHO1 is required for the formation of midbody matrix and the completion of cytokinesis in mammalian cells. Mol Biol Cell 13, 1832–1845.
Mierzwa B, Gerlich DW (2014). Cytokinetic abscission: molecular mechanisms and temporal control. Dev Cell 31, 525–538.
Mishima M, Kaitna S, Glotzer M (2002). Central spindle assembly and cytokinesis require a kinesin-like protein/RhoGAP complex with microtubule bundling activity. Dev Cell 2, 41–54.
Mollinari C, Kleman JP, Jiang W, Schoehn G, Hunter T, Margolis RL (2002). PRC1 is a microtubule binding and bundling protein essential to maintain the mitotic spindle midzone. J Cell Biol 157, 1175–1186.
Mollinari C, Kleman JP, Saoudi Y, Jablonski SA, Perard J, Yen TJ, Margolis RL (2005). Ablation of PRC1 by small interfering RNA demonstrates that cytokinetic abscission requires a central spindle bundle in mammalian cells, whereas completion of furrowing does not. Mol Biol Cell 16, 1043–1055.
Motegi F, Velarde NV, Piano F, Sugimoto A (2006). Two phases of astral microtubule activity during cytokinesis in C. elegans embryos. Dev Cell 10, 509–520.
Murata-Hori M, Wang YL (2002). Both midzone and astral microtubules are involved in the delivery of cytokinesis signals: insights from the mobility of aurora B. J Cell Biol 159, 45–53.
Murthy K, Wadsworth P (2008). Dual role for microtubules in regulating cortical contractility during cytokinesis. J Cell Sci 121, 2350–2359.
Nishimura Y, Yonemura S (2006). Centralspindlin regulates ECT2 and RhoA accumulation at the equatorial cortex during cytokinesis. J Cell Sci 119, 104–114.
Nislow C, Lombillo VA, Kuriyama R, McIntosh JR (1992). A plus-end-directed motor enzyme that moves antiparallel microtubules in vitro localizes to the interzone of mitotic spindles. Nature 359, 543–547.
Petronczki M, Glotzer M, Kraut N, Peters JM (2007). Polo-like kinase 1 triggers the initiation of cytokinesis in human cells by promoting recruitment of the RhoGEF Ect2 to the central spindle. Dev Cell 12, 713–725.
Piekny AJ, Glotzer M (2008). Anillin is a scaffold protein that links RhoA, actin, and myosin during cytokinesis. Curr Biol 18, 30–36.
Rankin KE, Wordeman L (2010). Long astral microtubules uncouple mitotic spindles from the cytokinetic furrow. J Cell Biol 190, 35–43.
Rappaport R (1961). Experiments concerning the cleavage stimulus in sand dollar eggs. J Exp Zool 148, 81–89.
Somers WG, Saint R (2003). A RhoGEF and Rho family GTPase-activating protein complex links the contractile ring to cortical microtubules at the onset of cytokinesis. Dev Cell 4, 29–39.
Steigemann P, Wurzenberger C, Schmitz MH, Held M, Guizetti J, Maar S, Gerlich DW (2009). Aurora B-mediated abscission checkpoint protects against tetraploidization. Cell 136, 473–484.
Straight AF, Field CM, Mitchison TJ (2005). Anillin binds nonmuscle myosin II and regulates the contractile ring. Mol Biol Cell 16, 193–201.
Su KC, Takaki T, Petronczki M (2011). Targeting of the RhoGEF Ect2 to the equatorial membrane controls cleavage furrow formation during cytokinesis. Dev Cell 21, 1104–1115.
Tatsumoto T, Xie X, Blumenthal R, Okamoto I, Miki T (1999). Human ECT2 is an exchange factor for Rho GTPases, phosphorylated in G2/M phases, and involved in cytokinesis. J Cell Biol 147, 921–928.
Uehara R, Goshima G (2010). Functional central spindle assembly requires de novo microtubule generation in the interchromosomal region during anaphase. J Cell Biol 191, 259–267.
Uehara R, Nozawa RS, Tomioka A, Petry S, Vale RD, Obuse C, Goshima G (2009). The augmin complex plays a critical role in spindle microtubule generation for mitotic progression and cytokinesis in human cells. Proc Natl Acad Sci USA 106, 6998–7003.
Uehara R, Tsukada Y, Kamasaki T, Poser I, Yoda K, Gerlich DW, Goshima G (2013). Aurora B and Kif2A control microtubule length for assembly of a functional central spindle during anaphase. J Cell Biol 202, 623–636.
van Oostende Triplet C, Jaramillo Garcia M, Haji Bik H, Beaudet D, Piekny A (2014). Anillin interacts with microtubules and is part of the astral pathway that defines cortical domains. J Cell Sci 127, 3699–3710.
Verbrugghe KJ, White JG (2004). SPD-1 is required for the formation of the spindle midzone but is not essential for the completion of cytokinesis in C. elegans embryos. Curr Biol 14, 1755–1760.
von Dassow G, Verbrugghe KJ, Miller AL, Sider JR, Bement WM (2009). Action at a distance during cytokinesis. J Cell Biol 187, 831–845.
Watanabe S, Ando Y, Yasuda S, Hosoya H, Watanabe N, Ishizaki T, Narumiya S (2008). mDia2 induces the actin scaffold for the contractile ring and stabilizes its position during cytokinesis in NIH 3T3 cells. Mol Biol Cell 19, 2328–2338.
Watanabe S, Okawa K, Miki T, Sakamoto S, Morinaga T, Segawa K, Arakawa T, Kinoshita M, Ishizaki T, Narumiya S (2010). Rho and anillin-dependent control of mDia2 localization and function in cytokinesis. Mol Biol Cell 21, 3193–3204.

Wei Q, Adelstein RS (2000). Conditional expression of a truncated fragment of nonmuscle myosin II-A alters cell shape but not cytokinesis in HeLa cells. Mol Biol Cell 11, 3617–3627.
Werner M, Munro E, Glotzer M (2007). Astral signals spatially bias cortical myosin recruitment to break symmetry and promote cytokinesis. Curr Biol 17, 1286–1297.
Wolfe BA, Takaki T, Petronczki M, Glotzer M (2009). Polo-like kinase 1 directs assembly of the HsCyk-4 RhoGAP/Ect2 RhoGEF complex to initiate cleavage furrow formation. PLoS Biol 7, e1000110.
Wu G, Lin YT, Wei R, Chen Y, Shan Z, Lee WH (2008). Hice1, a novel microtubule-associated protein required for maintenance of spindle integrity and chromosomal stability in human cells. Mol Cell Biol 28, 3652–3662.
Yoshigaki T (1999). Simulation of density gradients of astral microtubules at cell surface in cytokinesis of sea urchin eggs. J Theor Biol 196, 211–224.
Yuce O, Piekny A, Glotzer M (2005). An ECT2-centralspindlin complex regulates the localization and function of RhoA. J Cell Biol 170, 571–582.
Zhao WM, Seki A, Fang G (2006). Cep55, a microtubule-bundling protein, associates with centralspindlin to control the midbody integrity and cell abscission during cytokinesis. Mol Biol Cell 17, 3881–3896.